RESEARCH ON THE INFLUENCE OF Al_2O_3 AND TiO_2 OXIDE ADDITIVES ON ENAMEL ADHESION, BY IMPACT TESTING

Mihăiţă IOAN[1], Ramona-Nicoleta TURCU[2*], Roxana TRUSCĂ[3], Eugen Cătălin SFĂT[4], Mihai TÂRCOLEA[5]

The influence of the mill additions with refractory properties, Al_2O_3 and TiO_2, has been investigated in a TBC enamel, using the impact testing method. The deposit support was a non-alloy steel with low carbon content. The paper presents the analysis of the variation in the impact resistance of the deposited layers, with different mill additions. The novelties presented in the paper are: the nature of the mill additions, their influence on the coating adhesion and experimental data resulting from the computer processing of optical microscopy images, for the quantitative estimation of the layer adhesion. It is concluded that the adhesion varies significantly with the nature and content of mill additives, thus allowing adhesion control by selective use of mill additives.

Keywords: Enamel adhesion, thermal barrier, impact test, microcomposite refractory enamel, adhesion index

1. Introduction

The great variety of available glass enamel compositions and the possibility of modeling their properties, creates the premise for their use in a wide range of applications, depending on their composition, the nature and properties of the used support [1-4].

Thermal barrier coatings (TBC) enamels are deposited on metal supports to protect them from the action of temperature variations, given their thermal insulation properties [4-9]. Glass enamels that exhibit superior technical properties such as high temperature resistance, thermal stability, high hardness, abrasion resistance and

[1] PhD Candidate, Faculty of Materials Science and Engineering, University POLITEHNICA of Bucharest, Romania, e-mail: mihaita.ioan@gmail.com;
[2*] PhD Eng., Metallic Materials Science & Physical Metallurgy Department, University POLITEHNICA of Bucharest, Romania, e-mail: ramona.turcu@upb.ro;
[3] Senior researcher, FILS, University POLITEHNICA of Bucharest, e-mail: truscaroxana@yahoo.com;
[4] Prof., Faculty of Materials Science and Engineering, University POLITEHNICA of Bucharest, Romania, e-mail: sfateugen@yahoo.com;
[5] Prof., Metallic Materials Science & Physical Metallurgy Department, University POLITEHNICA of Bucharest, Romania, e-mail: mihai.tarcolea@upb.ro

chemical stability are frequently preferred as coatings for improving the surface properties of metallic materials and increasing their resistance to corrosion and erosion. There are many components that are exposed both to high temperatures, in the range of 900-1200^0 C, and sudden temperature variations (thermal shock) in the operation of heat engines [5]. Also, given the exhaust processes of the combustion gases, which also contain solid particles in suspension, the stresses are also manifested on the level of their mechanical action on the deposited layers, in the form of an erosive process [10]. In addition to these requirements, TBC coatings must also exhibit corrosion resistance, chemical stability at high temperatures and certain mechanical characteristics. This whole complex of requirements is definitely related to the adhesion of the coating to the substrate. Additives such as aluminium oxide, zirconium oxide, cerium oxide, lead oxide, and titanium oxide are useful for enhancing some properties mentioned above [1, 11-13]. In the literature, there are data on the evaluation of coating characteristics such as plasticity, adhesion strength [14, 15], impact abrasion resistance [7,16-18] or hardness [19-21].

Based on the above-mentioned, the paper addresses the influence of Al_2O_3 and TiO_2 oxide additives on enamel adhesion using the impact test method. The behaviour of the specimen to the impact test was investigated through optical microscopy (OM) and SEM-EDS. Subsequently, the imprint of impact test was analysis using Image Pro-Materials Pro software, Media Cybernetics. The adhesion index was estimated according to EN 10209 standard. The compositions of the support and of the coating were measured by optical spectrometry and ED-XRF, respectively.

The novelties presented in the paper are: 1) the nature of the mill additions; 2) the mill addition influences on the coating adhesion; 3) experimental data regarding the quantitative estimation of the layer adhesion.

2. Materials and methods

2.1 Sample preparation

The support of the enamels consists of low alloy steel whose elemental composition is presented in table 1. The enameled specimen undertaken impact test were prepared according to EN ISO 28764: 2015 [22]. The chemical composition was estimated by UV-VIS optical emission spectroscopy using a SPECTROMAXx LMM004 spectrometer. The expanded uncertainty having 95% confidence level, U (95%), assigned to the measurement data is presented in Table 1.

Table 1.

Chemical analysis of the steel substrate

Elements	C	Mn	P	S	Si	Cr	Ni	Al	Cu	Fe
% mass	0.05	0.22	0.013	0.009	0.008	0.02	0.03	0.06	0.03	rest
U(95%)	0.004	0.07	0.006	0.002	0.002	0.003	0.003	0.005	0.003	-

Discs made of 0.5 mm thick, and 60 mm diameter were cut from the mentioned steel. The discs were cleaned by blasting with 9.2 Mohs electro-corundum powder,

grain size 80-140 Mesh ASTM-E11 and then with compressed air, then degreased with ethyl alcohol, after which they were oven dried for 10 minutes at 60-80^0 C.

The frit contained alkaline elements, for an optimal correlation with the thermal expansion of the steel, as well as oxides with a good adhesion to the substrate, to increase the adhesion of the enamel coating. The frit was ground and homogenized, then chemically analyzed by X-ray fluorescence using an AMETEK SPECTRO XEPOS-03 spectrometer. The estimated chemical composition is presented in Table 2.

Table 2.

Chemical analysis of frit basic recipe

Oxide	SiO_2	Na_2O	CuO	Fe_2O_3	Al_2O_3	CaO	CoO	TiO_2	K_2O	MnO	Cr_2O_3
% mass	46.11	12.16	6.53	6.10	1.56	5.03	4.49	1.07	3.91	2.87	1.14

Impact resistance tests were performed on 1 sample coated with the basic recipe and 6 enamel-coated samples in which 3 samples have the enamel coating derived from the basic recipe with Al_2O_3 additive and 3 samples have the enamel coating derived from the basic recipe, with TiO_2 additive. In both cases, the additives were in percentages of 3, 5, and 8% of the basic frit.

Al_2O_3 powder, MERCK quality, granulation 70-230 mesh ASTM-E11, was chosen for its thermal insulation and refractory characteristics. TiO_2 powder, HERMAN quality, granulation 80-300 mesh ASTM-E11, was chosen for its surfactant and thermal insulation properties. The corresponding sample coding is shown in Table 3 and Table 4.

Table 3.

Coding of Al_2O_3-added samples

Sample code	Frit (% of mass)	Addition Al_2O_3
B	100	0
BAL3	97	3
BAL5	95	5
BAL8	92	8

Table 4.

Coding of TiO_2-added samples

Sample code	Frit (% of mass)	Addition TiO_2
B	100	0
BTI3	97	3
BTI5	95	5
BTI8	92	8

2.2 Impact test

The impact test was carried out based on ISO 4532 and using the device, in accordance with EN-ISO 6271, DIN 55669 and EN-ISO 10209-C. The impact mass used was 1.5 kg and the impact tip had a diameter of 22 mm. The drop height was 600 mm according to ISO 10209. The test conditions were the same for all prepared samples.

The impact adhesion was assessed according to the classification system presented in the BS EN 10209 standard. This standard provides for 5 classes of adhesion after the impact test, which refer to the way the enamel coating breaks in the deformed area, starting from Class 1, excellent adhesion, up to Class 5, very poor adhesion. The adhesion can be judged by comparing the images obtained by the impact test with the images from the reference photographs in the standard.

The impact cracking and fracture patterns can be classified according to the ratio R/t, where R is the radius of curvature of the impact cavity and t is the thickness of the deposited layer [23]. Three crack patterns can thus be identified: circular and concentric cracks occurring at the periphery of the formed cavity, channel cracks occurring inside the formed cavity and radial cracks starting from the center of the formed cavity and propagating straight outwards [7, 24-26].

3. Results

3.1 X-ray fluorescence analysis

After adding the oxides, the resulting enamels were analyzed by XRF spectrometry, the results are shown in Fig. 1 (BAL samples) and 2 (BTI samples).

The results of XRF spectrometric analysis confirm that the predicted recipes are obtained.

CODE	BAl3	BAl5	BAl8
Symbol	%wt	%wt	%wt
Na2O	6.015	5.747	4.188
Al2O3	4.1	5.093	7.78
SiO2	35.05	34.49	27.58
K2O	2.971	2.879	2.249
CaO	3.831	3.669	2.894
TiO2	3.036	2.947	2.27
Cr2O3	0.8518	0.8725	0.7787
MnO	2.813	2.84	2.24
Fe2O3	4.517	4.548	3.493
CoO	3.277	3.182	2.595
CuO	4.727	4.699	4.206

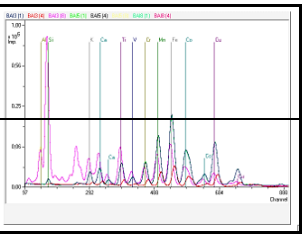

Fig. 1. Results of XRF spectrometric analysis of BAL samples

CODE	BTI3	BTI5	BTI8
Symbol	%wt.	%wt.	%wt.
Na2O	5.795	6.759	4.452
Al2O3	4.205	5.821	7.861
SiO2	42.56	45.79	41.2
K2O	2.81	2.57	2.36
CaO	3.672	3.293	3.13
TiO2	5.063	10.33	13.21
Cr2O3	0.8116	0.8755	0.82
MnO	2.80	2.44	2.535
Fe2O3	4.418	3.877	4.056
CoO	3.301	2.924	3.055
CuO	4.543	4.315	4.361

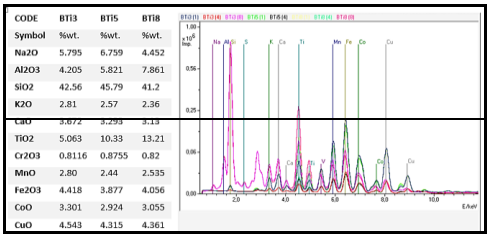

Fig. 2. Results of XRF spectrometric analysis BTI samples

For each of the six recipes, the slurry was prepared by mixing the ground frit with 40% water, corresponding to a density of 1.70-1.72 g/cm^3. The mixture was stirred for 5 minutes and applied by wet spraying onto the metal surface. After coating, the samples were air dried at a temperature of 20-30^0 C for 30 minutes and then oven dried at 70-100^0 C for 60 minutes. The samples were burned in an electric oven at 860^0 C, for 3 minutes.

3.2 Optical microscopy

Impact-tested samples were analyzed by stereoscopic light microscopy using an Olympus SZX-7 microscope equipped with a Hitachi KP-D50 camera.

Light microscopy images of the BAL and BTI impact samples are shown in Fig. 3 (b, c, d) and Fig. 3 (f, g, h) respectively, together with the "control sample" B in Fig. 3 (a, e).

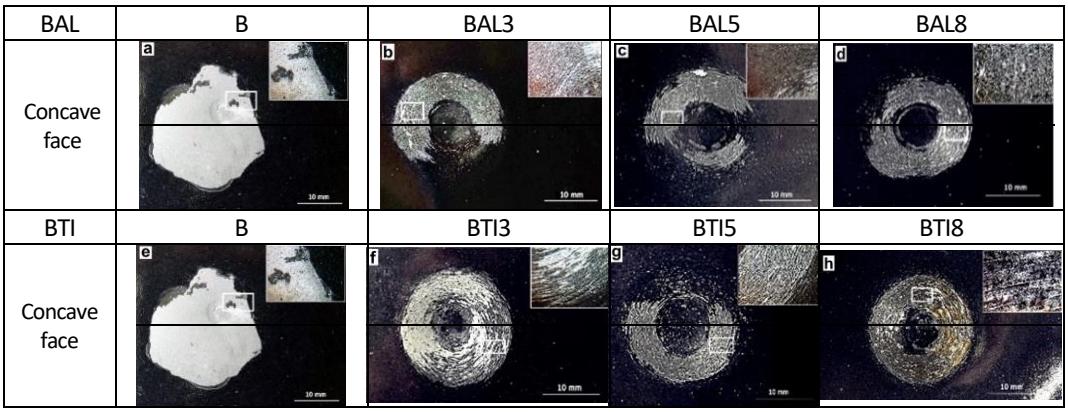

Fig. 3. Optical microscopy images of impact test specimens

From the analysis of the optical microscopy images of the samples subjected to impact, characteristic aspects related to cracking, peeling or detachment of the enamel layers following plastic deformation of the coated substrate are observed. BAL samples show both surface cracks without substrate exposure and perforated cracks with metal substrate exposure. It is observed that in BAL3 and BAL8 samples the cracking occurs over most of the impact crater as circular cracks concentric with the center of the impact cavity. The character of the cracks is mostly penetrating, with exposure of the substrate and large areas of complete enamel detachment. Sample BAL5 shows smaller cracked areas than samples BAL3 and BAL8, and the cracks are mostly shallow without exposing the substrate. Sample B shows a total removal of the enamel layer over approximately 90% of the concave impact zone.

The light microscopy images obtained on the BTI samples reveal generally the same features as the BAL samples, i.e. areas of shallow cracks and perforated cracks, accompanied by areas where the enamel has been completely removed. In comparison, BTI5 and BTI8 samples are found to have better impact resistance compared to B and BTI3 samples. Based on adhesion performance classification according to EN 10209 it can be concluded that samples BAL3, BAL8, BTI3 and BTI5 fall into class 3 (Medium: impact surface slightly covered by enamel layer with large areas of visible substrate) or Class 4 (Poor: impact surface shows little trace of enamel layer). Samples BAL5 and BTI8 can be classified as Class 2 (Very good: the impact surface is largely covered by cracked enamel, with small areas of visible substrate), while "control" samples B fall into Class 5 (Very poor: the impact surface is completely free of enamel, with a clear boundary between the layer and the substrate) (Fig. 3).

In terms of the arrangement on the surface of the impact cavity, from the details shown, it can be seen that the surface cracks are located on the edge of the cavity, and as they approach the center of the cavity, the perforated (penetrating) cracks become predominant (majority). In the central area of the impact cavity, the simultaneous presence of circular, radial and groove cracks is observed, without detaching the enamel

layer. This pattern is due to the local plastic deformation scheme of the "substrate-coating" system (Fig. 4), which on the concave face is tensile bending for the enamel layer and compressive bending for the substrate (S1).

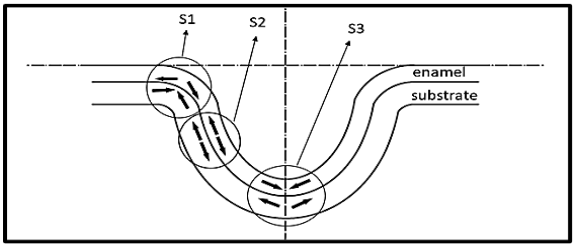

Fig. 4. Arrangement of local plastic deformation scheme on the impact cavity profile.

In the intermediate area of the cavity, the pattern is tensile bending for the entire "substrate-enamel" system (S2), and in the central area of the impact cavity, the plastic deformation pattern is compressive bending for the enamel and tensile bending for the substrate (S3).

Using optical microscopy images, the size of the area with intact layer and surface cracks and the area with penetrating cracks and layer detachments was determined. Determinations were made by image analysis using Image Pro-Materials Pro software from Media Cybernetics. The analyzed images were processed with specialized software and are shown in Fig. 5.

BAL	B	BAL3	BAL5	BAL8
Concave face processing	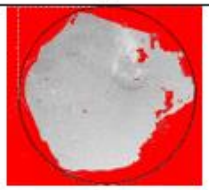	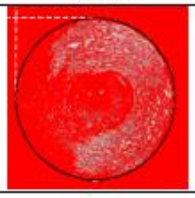	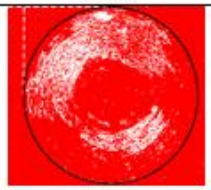	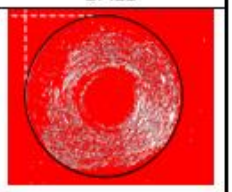
	a.	b.	c.	d.
BTI	B	BTI3	BTI5	BTI8
Concave face processing	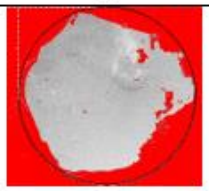	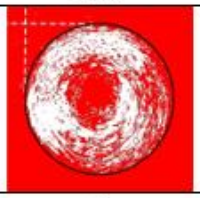	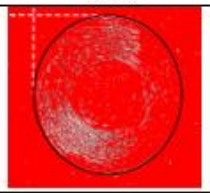	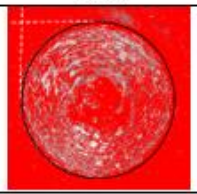
	e.	f.	g.	h.

Fig. 5. Processing of analyzed images

The results of the image analyze on the impact tested samples are presented in Tables 5 (BAL) and 6 (BTI) (the weights of the significant areas inside the circle that delimit the concave area of the impact cavity are presented).

Table 5

Important area weights for BAL samples

Code	Detached Area, D (%)	Adherent Area , A (%)	Ratio A/D
B	73.14	26.86	0.37
BTI3	34.98	65.02	1.86
BTI5	26.72	73.28	2.74
BTI8	18.97	81.03	4.27

Table 6

Important area weights for BTI samples

Code	Detached Area, D (%)	Adherent Area,A (%)	Ratio A/D
B	73.14	26.86	0.37
BAL3	25.04	74.96	2.99
BAL5	20.81	79.19	3.80
BAL8	27.44	72.56	2.64

Also, for the two series of tests, the values of the ratio between the adherent area (A) and the detached area (D) are presented.

3.2 SEM Microscopy

The impact test samples were also analyzed by SEM microscopy using a QUANTA INSPECT F 50 scanning electron microscope equipped with a field emission gun (FEG) with a resolution of 1.2 nm and an energy dispersive X-ray spectrometer (EDS) with a MnKα resolution of 133 eV. The SEM investigations were carried out on cross-sections in the area of maximum curvature of the impact cavity and revealed the presence of shallow and penetrating cracks, isolated or intercommunicating, oriented according to the local stress pattern as it can be seen in Fig. 4 (Fig. 6).

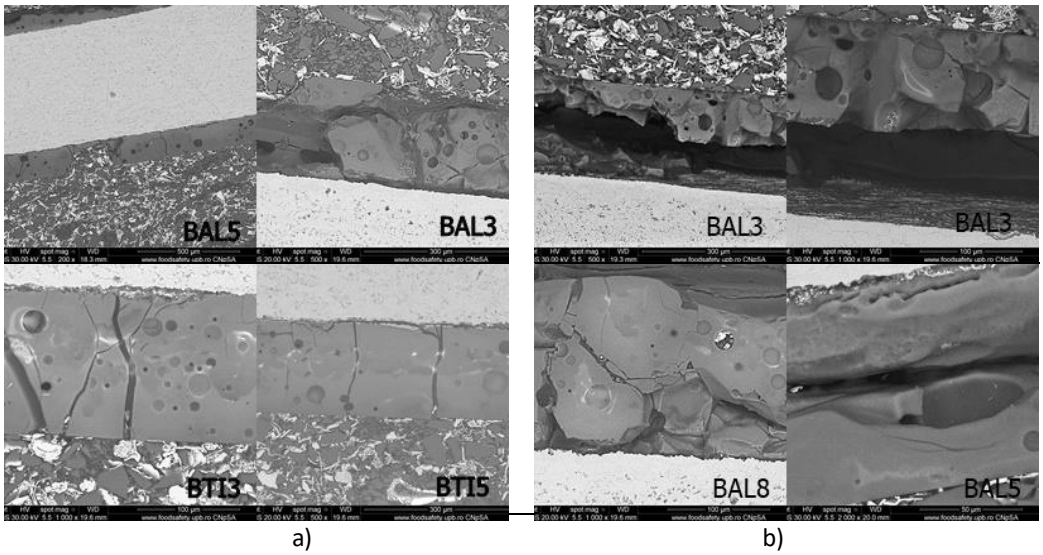

a) b)

Fig. 6.1. SEM images represents the appearance of cracks in areas: a) areas with S1 local deformation pattern; b) areas with S2 local deformation pattern

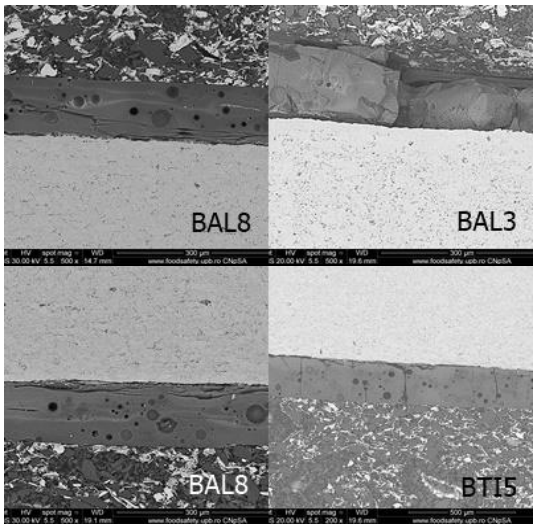

c)

Fig. 6.2. SEM images represents the appearance of cracks in areas: c) areas with S3 stress schemes

In the areas according to the S1 pattern, penetrating cracks and shallow cracks are observed, radially oriented, according to the local curvature (Fig. 6.a). The SEM image in Fig. 6.b represents the cracks according to the S2 pattern. Longitudinal cracks and penetrating transverse cracks as well as areas with a detached layer are highlighted. In the S3 areas (Fig. 6.c), SEM images show mainly shallow cracks, with no substrate visible.

4. Discussion

Research has focused on estimating the effects of aluminum oxide (Al_2O_3) and titanium oxide (TiO_2), as frit additives, on the adhesion of the enamel layer deposited on a non-alloy steel support. Six different enamel recipes were elaborated, starting from a classic "thermal barrier coating" (TBC) type enamel composition, to which were added, when mill the frit, the two oxides in different proportions, of 3, 5 and 8% by weight, for each one.

The samples were subjected to the impact test, according to ISO 4532, and the cavities obtained were investigated by optical microscopy, computer image processing and SEM electron microscopy. The impact test was performed on a device according to the BS EN 10209. Optical microscopy images of impact cavity have highlighted classic elements of impact testing, namely areas with an enamel layer, cracked areas and areas of total detachment of the layer. Taking into account the mechanics of the plastic deformation process of the "enamel-substrate" system, three local stress schemes were identified on the contour of the impact profile (Fig. 4). It is found that the most favorable application scheme in terms of layer adhesion is S3, with compression for

enamel and tensile forces for substrate. The cracks in the three characteristic areas have specific aspects, depending on how the enamel-substrate system reacts to locally acting forces generated by the impact test. Thus, in the areas on the edge of the impact trace, where predominate S1 scheme, the optical microscopy studies (Fig. 3 b, f, g) revealed that the bending of the enamel layer determined the predominant appearance of the circular cracks concentric with impact cavity. SEM electron microscopy studies (Fig. 6), on cross-sections of samples, showed that the cracks in these areas are both superficial and penetrating, with partial exposure of the substrate. In the intermediate areas of the impact cavity, corresponding to S2 scheme, the optical microscopy (Fig. 3 h, c) and the SEM electron microscopy (Fig. 6.b) confirmed the majority presence of longitudinal cracks and penetrating transverse cracks, alternating with areas stretched by the detached layer. Optical microscopy and SEM electron microscopy studies have confirmed that the areas with S3 application schemes have the highest percentage of areas with an adherent layer, corresponding to the bottom of the impact cavity. The existence of longitudinal cracks located in the middle of the enamel layer indicates that the internal cohesive forces of the enamel are exceeded by the adhesion forces of the layer to the substrate, while the longitudinal cracks located at the layer-substrate interface show that the internal resistance of the enamel is higher than the adhesion forces. The processing of optical microscopy images with the Image Pro-Materials Pro software allowed the development of an analysis procedure capable to determine the size of the surfaces with adhered layer and those with detached layer (Tables 5 and 6). In the Figs. 7 and 8 are represented the graphs related to the variation of significant areas corresponding to the BAL and BTI samples. These allowed the calculation of the Adhesion Index, as a share of the area with adhesive layer, in the total surface of the impact cavity.

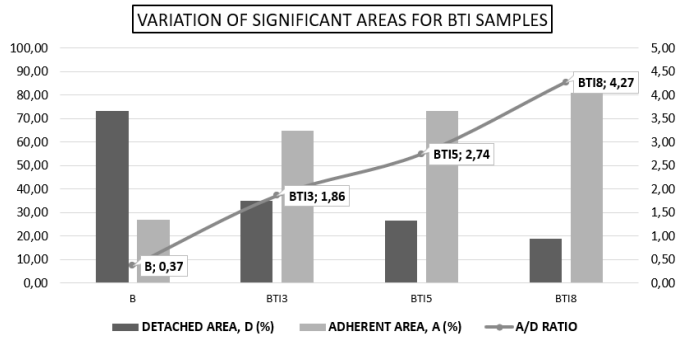

Fig. 7. The variation of significant areas for BAL samples

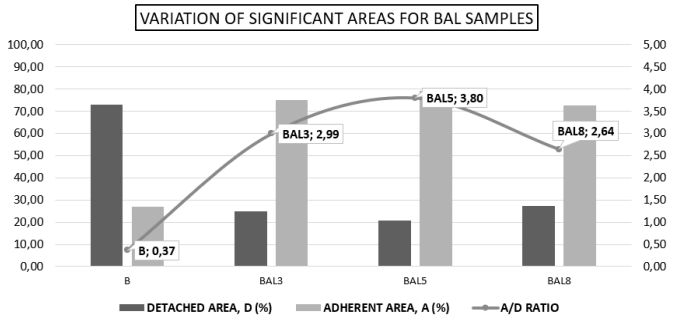

Fig. 8. The variation of significant areas for BTI samples

The variation of the adhesion index with the variation of the mill addition content is presented in Fig. 9, for the samples with added Al_2O_3 and for the samples with added TiO_2.

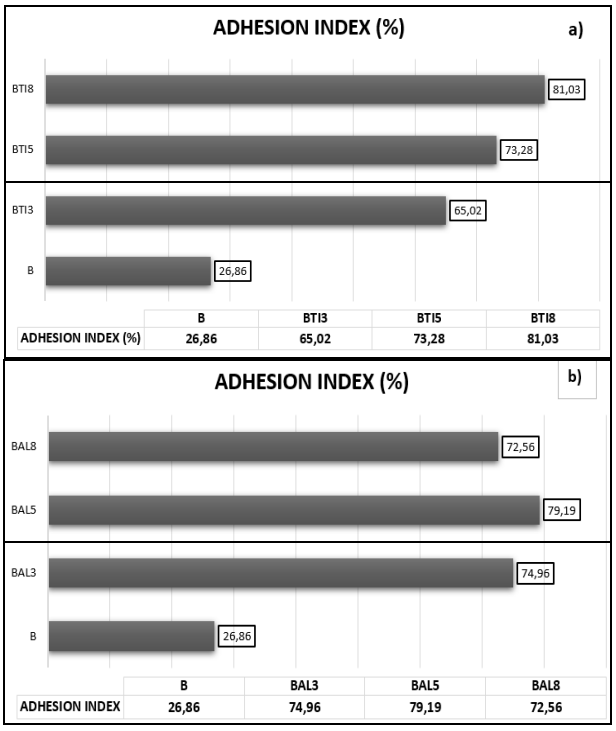

Fig. 9. Variation of adhesion index a) BTI samples b) BAL samples

It can be seen in Fig. 9 that the significant areas and the adhesion index are strongly influenced by the presence of the two mill additions, with samples BAL and BTI showing much better results than sample B. The results also show that the variation in the mill additive content generates variations in the adhesion of the enamel to the substrate, with the best results showing the BAL5 and BTI8 samples.

5. Conclusion

TBC enamels modified by the addition of Al_2O_3 and TiO_2, oxides with refractory and insulating properties, showed significant increases in adhesion to the unalloyed carbon steel substrate. The deposition adhesion to the substrate was studied by impact test, according to ISO 4532, performed on samples with different recipes of TBC-type enamels modified with 3, 5, 8% mill additives. Optical microscopy and SEM electron microscopy studies showed that certain categories of cracks appeared in different areas of the impact cavity, depending on the mechanical stress pattern present in that area. The shape and orientation of the cracks primarily take into account the mechanics of the local plastic deformation process, but also the percentage of mill additives. In this way, it was possible to establish a correlation between the impact tested samples and the adhesion classes provided by EN 10209, thus proposing a quantitative interpretation of the adhesion classes mentioned in EN 10209.

For Al_2O_3 recipes there is a variation along a curve with a maximum point for the 5% oxide addition sample, and for TiO_2 recipes, the best adhesion is shown by the 8% oxide addition sample.

The novelty brought by this research is the quantitative evaluation of adhesion by calculating the adhesion index, using optical microscopy image analysis and processing, with the Image Pro-materials software, which complements the provisions of EN 10209 standard, concerning the qualitative classification of impact tested deposited coatings. Further research will address the influence of mill additives on the thermal barrier effects and thermal shock resistance characteristics of these enamel coatings.

REFERENCES

[1]. *S. Rossi, F. Russo, M. Calovi,* Durability of vitreous enamel coatings and their resistance to abrasion, chemicals, and corrosion: a review, Journal of Coatings Technology and Research **Vol. 18**, 2021, pp. 39–52.

[2]. *S. Rossi, F. Russo, N. Gasparre, V. Fontanari,* Influence of graphene addition on the mechanical and surface properties of vitreous enamel coatings, Surface and Coatings Technology, **Vol. 398**, 2020.

[3]. *T. O. Soshina, V. R. Mukhamadyarova,* On the defects of enamel coatings, January **2019**, Voprosy Materialovedeniya, DOI: 10.22349/1994-6716-2018-96-4-145-150.

[4]. *F. Russo, V. Fontanari, S. Rossi,* Abrasion behavior and functional properties of composite vitreous enamel coatings fabricated with the addition of 316L stainless steel flakes - Ceramics International, 2022 – Elsevier, Available online 7 May **2022**, Version of Record 22 June 2022.

[5]. *L.V. Klimova, A.V. Ryabova, V.V. Kerimova,* Chemically Resistant Glass-Enamel Coating for the Protection of Steel Pipelines, Materials Science Forum, May 2020**, 992**: 598-604.

[6]. *M. Branzei, I. Pencea, A. A. Matei, C.E. Sfat, I. V. Antoniac, R. N. Turcu, V. Manoliu*, Influence of high temperature exposure on the adhesion of a micro-composite refractory enamel to a Ni-18-Cr-12W superalloy, J. of Adhesion Science & Technology, **Vol. 31**, 2017**,** p. 2555-2570.

[7]. *H Qian, S Chen, T Wang, G Cheng, X Chen*, Silicon nitride modified enamel coatings enable high thermal shock and corrosion resistances for steel protection, Surface and Coatings Technology, **Vol. 421**, 127474, 2021.

[8]. *R.N. Turcu, I. Pencea, G. Chisiu, V. Manoliu, M. Botan, M. Branzei, F. Niculescu, A. C. Popescu-Arges, M. Ioan, C.E. Sfat,* Roughness and were resistance modification induced by cyclic

temperature shicks upon a micro-composite refractory enamel, U.P.B. Sci. Bull., Series B, **Vol. 82**, Iss. 4, 2020, pg.223-234.

[9]. *Y.Liao, M.Chen, M.Feng, Q.Wang, J.Wang, S.Zhu, F.Wang*, Thermal shock and self-healing behavior of the enamel composite coatings with addition of various nanoparticles at temperatures of 700 and 800 °C, Corrosion Science, **Vol. 191**, October 2021.

[10]. *I.G. Berdzenishvili*, Protective Glass Coatings for Chemical Equipment, Pipes and Pipelines, Georgian Technical University, Tbilisi, **2008**.

[11]. *Ghazi K. Saeed, Ibtihal Alnamie , Sabah Abdual Noor* , Effect of Different Percentages of Titanium Dioxide Additives on the Enamel Protecting of Steel Surface, Iraqi Journal of Science, 2014, **Vol 55**, No.2A, pp:435-443

[12]. *Chaozheng Fan, Lida Luo, Qingwei Wang and Weizhong Jiang*, Effect of CeO_2 on Enamel Coatings on the Surface of Corten Steel, IOP Conf. Series: Materials Science and Engineering **562**, 2019, 012008.

[13]. *Stefano Rossi, Caterina Zanella, Ryan Sommerhuber*, Influence of mill additives on vitreous enamel properties, Materials & Design, **Vol. 55**, 2014, Pages 880-887.

[14]. *I.K.Abdulrahman, I.A.Mahmood,A.S.Jabor*, Effects of heat treatment, quartz additions and particle size on the properties of enamel with low-alloy steel substrate, IOP Publishing Ltd, IOP Conference Series: Materials Science and Engineering, **Vol. 671**, November 2019.

[15]. *R Pérez, A Querejeta, MÁ Corres, J Munoz,* Thermal behaviour of vitreous ceramic coatings obtained by electrophoretic deposition for furnace components, Ceramics International, **Vol. 46**, Issue 13, 2020, pp. 20695-20706.

[16]. *K.Xu, H.Xue, J.Zheng, A,Wang, L.Zhang, J.Liu,* Improving the mechanical impact and bending resistances of enamel via B_2O_3 addition, Ceramics International,**Vol. 47**, Issue 19, **2021**, pp. 27195-27200

[17]. *C. Rebholz, H. Ziegele, A. Leyland, A. Matthews*, Structure, mechanical and tribological properties of nitrogen-containing chromium coatings prepared by reactive magnetron sputtering, Surf. Coat. Technol. **115**, 1999, pp. 222-229.

[18]. *K.-D. Bouzakis, A. Asimakopoulos, N. Michailidis, S. Kompogiannis, G. Maliaris, G., Giannopoulos, E. Pavlidou, G. Erkens*, The inclined impact test, an efficient method to characterize coatings' cohesion and adhesion properties, Thin Solid Films **Vol. 469–470**, 2004, pp. 254-262.

[19]. *K.-D. Bouzakis, A. Asimakopoulos, G. Skordaris, E. Pavlidou, G. Erkens*, The inclined impact test: A novel method for the quantification of the adhesion properties of PVD films, Wear **Vol. 262**, I. 11-12, 2007, pp. 1471.

[20]. *A. Faeghinia, E. Jabbari*, Suitable Na2O-SiO2, BaO-SiO2 Based Coatings for Stainless Steels, Journal of Materials and Applications, **Vol 10**, No. 2, **2021**.

[21]. *P.Mukherjee, P.Roy, S.Ghosh*, Study about Fabrication and Evaluation of Different Thermal Barrier Coating Systems, Research Developments in Science and Technology **Vol. 1**, 6 April **2022** , pp. 57-64, doi 10.9734/bpi/rdst/v1/2726C.

[22]. EN ISO 28764:2015, Émaux vitrifiés - Production d'éprouvettes pour l'essai des émaux sur la tôle d'acier, la tôle d'aluminium et la fonte.

[23]. *D. Mercier, V. Mandrillon, G. Parry, M. Verdier, R. Estevez, Y. Bréchet, T. Maindron*, Investigation of the fracture of very thin amorphous alumina film during spherical nanoindentation. Thin. Solid. Films **2017,** 638, pp. 34–47

[24]. *M. Krabbe,* Crack Mechanisms and Crack Interaction in Thin Films; Department of Engineering, Technical report ME-TR-1; Aarhus University **2012**; pp. 18–28, ISSN 2245-4594

[25]. *K. Fu, Y. Tang, L. Chang,* Toughness Assessment and Fracture Mechanism of Brittle Thin Films Under Nano-Indentation, Fracture Mechanics—Properties, Patterns and Behaviors; Intech Open: Rijeka, Italy, **2016**; pp. 121–144

[26] *D. Ben, S.P. Beake, J. F. Smith*, Evaluating the fracture properties and fatigue wear of tetrahedral amorphous carbon films on silicon by nano-impact testing, Surf. Coat. Technol. 177/178, 2004, 611